JOURNAL OF THE ROYAL SOCIETY Interface

J. R. Soc. Interface (2009) **6**, 1213–1221
doi:10.1098/rsif.2008.0021
Published online 11 March 2009

Nanoparticles of a different source induce different patterns of activation in key biochemical and cellular components of the host response

A. L. Guildford[1], T. Poletti[1], L. H. Osbourne[1], A. Di Cerbo[2], A. M. Gatti[2] and M. Santin[1,*]

[1]*School of Pharmacy & Biomolecular Sciences, University of Brighton, Brighton BN2 4GJ, UK*
[2]*Laboratorio Biomateriali, Dipartimento di Neuroscienze, Universita di Modena e Reggio Emilia, 41100 Modena, Italy*

Nanoparticulate materials are produced by industrial processing or engineered for specific biomedical applications. In both cases, their contact with the human body may lead to adverse reactions. Most of the published papers so far have focused on the cytotoxic effects of nanoparticles (NPs). Instead, the present *in vitro* study investigates the effect of different types of NP on key components of the host response such as clot formation and the inflammatory cells. The different NPs were pre-conditioned with platelet-rich human plasma for 30 min and then incubated with the blood mononuclear cells for 20 hours. The potential of the different NPs to induce clot formation, platelet activation and monocyte/macrophage differentiation was assessed by morphological analysis, immunocytochemistry and biochemical assays. The data showed that nanoparticulate materials based on antimony, silver and nickel were capable of promoting the polymerization of fibrin and the aggregation and fragmentation of platelets, leading to a moderately activated monocyte phenotype. This process was more pronounced in the case of antimony- and silver-based NPs that share a similar size and round-shaped morphology. Conversely, NPs of cobalt, titanium and iron appeared to stimulate cells to acquire a macrophage phenotype able to secrete higher levels of tumour necrosis factor α, a pro-inflammatory cytokine. Therefore, the present study provides clear indications about the subtle and adverse effects that the invasion of these materials may produce in the cardiovascular system and in vital organs.

Keywords: nanoparticles; inflammatory response; clot formation; macrophages; fibrin; platelets

1. INTRODUCTION

Nanomedicine has been sought as an opportunity to improve clinical treatments and diagnostics; it is reliant on nanostructured materials and nanodevices. Among the most used nanoscale materials, nanoparticles (NPs) have been considered as either drug carriers or contrast agents. For example, recent studies have highlighted that the use of iron oxide NPs as magnetic resonance imaging contrast agents leads to their phagocytosis by mononuclear cells via the macrophage 1 (MAC-1) receptor (van Zur Muhlen *et al.* 2006). This biological process has been exploited to detect resident macrophages in atherosclerotic lesions (Frias *et al.* 2008). Similarly, NPs have also been used for the prediction of the degree of inflammation in carotid atherosclerosis (Kooi *et al.* 2003) and for the detection of acute brain inflammation (McAteer *et al.* 2007). In a more sophisticated approach, iron oxide NPs functionalized by vascular cell adhesion molecule-1 ligands have been studied for the targeted detection of neovascularization in atherosclerotic lesions (Kelly *et al.* 2005). The broad range of NPs, their tuneable physico-chemical characteristics and, consequently, their ability to interact with biomolecules have also led to their exploitation in the field of nanosensors (Frias *et al.* 2006). However, NPs can also be accidentally generated as a result of industrial processes, causing environmental pollution, or they can be released *in vivo* from the wear and tear and/or corrosion of metallic biomedical implants. Regardless of their source and use, NPs can penetrate human tissues and accumulate as foreign bodies. As a consequence, an immune response is triggered, which may result in adverse reactions and pathological conditions. Indeed, NPs have been implicated in triggering potential toxicological and pathological conditions in cells and tissues (Kagan *et al.* 2005).

*Author for correspondence (m.santin@brighton.ac.uk).

Received 13 January 2009
Accepted 6 February 2009

Transition metals are known catalysts of oxidative stress in cells; oxidative species are generated which, interacting with metals, elicit redox-cycling cascades and tissue damage (Kagan *et al.* 2005). Metal ion NPs can also play a role as allergens, activating the host immune system. For example, different degrees of inflammatory response are thought to be activated depending on the NP size (Lucarelli *et al.* 2004). However, little has been investigated to date to link the different physico-chemical properties of the NP to the biochemical and cellular pathways of the host response.

In this paper, NPs that can potentially contact the human body as either technological tools or environmental contaminants have been tested for their ability to activate elements of the clotting system and human primary monocytes/macrophages (MMs). The study focused on specific biochemical pathways and cell morphological features, which may indicate the development of pro-inflammatory or post-inflammatory MM phenotypes (Martin & Leibovich 2005).

2. MATERIAL AND METHODS

Seven different types of NPs were selected and tested (table 1). The study investigated the immunological potential of three metal-based NPs, cobalt- (Co, Fluka, Germany), silver- (Ag) and nickel-based (Ni) (Nanoamor, USA) NPs and four ceramic oxide-based NPs, titanium- (TiO_2, Tal, USA), iron oxide- (Fe_2O_3 and Fe_3O_4) and antimony oxide-based (Sb_2O_3, Nanoamor, USA) NPs.

2.1. NP physico-chemical characterization

NP morphology and size were assessed by scanning electron microscopy (SEM; 6310 Jeol Instruments, UK). NPs were glued on stubs and SEM was performed at 20 kV and images were taken at 10 000× magnification. Average size values were assessed semi-quantitatively and compared with those reported by the NP manufacturers. Tendency to aggregation and surface nanotopography were also analysed.

2.2. Material-induced activation of host response components

Informed healthy blood donors ($n=10$) from both genders and in the age range of 21–50 were recruited, following written consent. The study was approved by the University of Brighton local research ethics committee. Heparinized venous peripheral blood samples (20 ml) were collected on different days and mononuclear cells were freshly isolated within 2 hours from vein puncturing using a Histopaque-1077 medium (Sigma, UK) by the Boyum method, as previously described (Santin *et al.* 2004). The cells were washed three times in phosphate-buffered saline pH 7.2 (PBS, Oxoid, UK) and re-suspended in Dulbecco's modified Eagle's medium (DMEM) enriched with 10 per cent (v/v) heat-inactivated foetal calf serum (FCS). Cell viability was assessed using trypan blue staining and was always found to be higher than 95 per cent. The cell isolation step also provided a fraction of platelet-rich plasma (PRP), which was collected and stored at room temperature in sterile conditions until use (approx. 30 min). PRP was used for preconditioning both the NP and the 24-well tissue culture plate (TCP) for 30 min. Mononuclear cells (1×10^5 cells ml^{-1}) were seeded onto a PRP pre-conditioned TCP and incubated for 3 hours at 37°C, in 5 per cent CO_2 and 95 per cent air. Meanwhile, 5 mg of each NP (table 1) was re-suspended in 10 per cent (v/v) FCS-supplemented DMEM and sonicated for 5 min. The medium was removed from the adhering mononuclear cells and the samples were washed three times by 10 per cent (v/v) FCS-supplemented DMEM and finally incubated in 1 ml of the same medium containing 0.05 mg ml^{-1} of the NP. NP-spiked samples were incubated overnight (20 hours) at 37°C, in 5 per cent CO_2 and 95 per cent air in static conditions. MMs adhering on PRP pre-conditioned TCP (Nunc, UK) were used as controls.

Table 1. NP chemical composition, size and use.

NP type	typical source	manufacturer	size (nm)
antimony oxide (Sb_2O_3)	industrial processes, paints, ceramics, etc.	Nanoamor, USA	41–91
silver (Ag)	antimicrobial coating	Nanoamor, USA	90–240
titanium oxide (TiO_2)	hip and dental coating	Tal, USA	20–160
cobalt (Co)	hip and stent material	Fluka, Germany	28
nickel (Ni)	stent material	Nanoamor, USA	62
Fe_3O_4	stent material	Nanoamor, USA	20–30
Fe_2O_3	stent material	Nanoamor, USA	55–65

2.2.1. Adhering cell SEM analysis, staining and immunocytochemistry. After 20 hours of incubation, adhering cells were washed three times in PBS and then fixed in 3.7 per cent (v/v) formaldehyde (Sigma, UK) in PBS. Following fixing, cell samples ($n=2$) were either prepared for SEM or processed for epifluorescence microscopy. Specimens for SEM were prepared by dehydration in increasing ethanol concentrations (25, 50, 75 and 90% by volume), air-dried, sputter-coated by palladium and finally analysed by SEM at 5 kV, at different magnifications. SEM analysis focused on MMs and platelet morphology as well as on their interactions with the NP. In particular, the degree of plasmalemma roughness and cell spreading was evaluated in the case of MMs, while aggregation and fragmentation were assessed in platelets. Wherever detectable, platelet analysis was associated with observations of NP-induced fibrin polymerization as a measure of the NP potential to induce clotting.

Staining by the phalloidin–rhodamine method was performed by making the cell membrane permeable to the dye by treatment in 0.1 per cent (w/v) Triton X-100 in PBS followed by incubation with phalloidin–tetramethylrhodamine-β-isothiocyanate (Sigma, UK)

for 30 min, at room temperature, under dark conditions. The samples were washed twice in PBS prior to final analysis at 40× magnification by a fluorescent inverted microscope (Eclipse TE2000-U, Nikon, UK) connected to a digital camera (D1x, Nikon, UK).

To confirm the presence of MM cells, the fixed samples were subjected to immunolabelling by CD68 antibody, a marker for both monocytes and macrophages. The samples were blocked for non-specific antibody binding in 4 per cent (w/v) bovine serum albumin for 30 min, incubated in 1 : 1000-diluted mouse monoclonal anti-CD68 solution (Vector Labs, UK) overnight at room temperature and were finally washed with an excess of PBS and incubated in anti-mouse AlexaFluor 548 tagged antibody (Invitrogen, UK) for 1 hour at room temperature. The samples ($n=3$) were analysed by inverted fluorescent microscope as described above. The morphology of MMs when incubated with the different NP and their marker expression were compared with that of control MMs adhering on plasma preconditioned TCP without any NP challenge.

2.2.2. Evaluation of NP-induced biochemical signalling and cytotoxicity in MMs. The supernatants from each experiment were collected and centrifuged at 1000*g* to eliminate any unbound cells and stored at −70°C until tested by ELISA kits for platelet-derived growth factor-BB (PDGF-BB) (PeproTech EC, UK, catalogue no. 900-K04), vascular endothelial growth factor (VEGF) (R&D Systems, UK, catalogue no. DVE00) and tumour necrosis factor α (TNFα) (Amersham, UK, catalogue no. RPN2781). TNFα secretion was evaluated as a marker of MM pro-inflammatory phenotype, while PDGF-BB and VEGF were tested to assess the cell potential to stimulate blood vessel formation (VEGF) and fibroblast proliferation (PDGF-BB) and, therefore, as markers of granulation and fibrous tissue formation. Standard curves with a linear coefficient no lower than 0.99 were obtained in triplicate by the kit's pure growth factor standards. Absorbance readings from the blank (10% FCS-enriched tissue culture medium) were subtracted from the sample values and data were expressed as pg ml^{-1} mean ± s.d. from $n>5$.

Cytotoxicity was evaluated by lactate dehydrogenase (LDH) activity assay of the supernatants using the Cytotox 96 kit (Promega, UK; Lewinski *et al.* 2008). The assay measures cell LDH activity via the oxidation of NADH to NAD^+ in the presence of lactate and pyruvate. The enzyme activity was measured by reading the absorbance at 490 nm by spectrophotometer (ELx800 BioTek, UK). Positive controls were obtained from the measurement of the LDH activity liberated from the cytoplasm of Triton-lysed cells (1×10^5 cells ml^{-1}). Data were expressed as means ± s.d. of the enzymatic arbitrary units from $n=6$.

2.3. Statistical analysis

Data were statistically analysed by pair *t*-tests and by ANOVA (Tukey's test) to allow comparative analysis across the samples. Data analysis was performed by Minitab Release v. 15 software (MINITAB, YK) and samples were considered significantly different at either $p\leq0.01$ or $p\leq0.05$.

3. RESULTS AND DISCUSSION

The advent of nanotechnologies, especially in the medical field, and the impact of industrial processes on the release of nanoparticulate material into the environment open new frontiers in the study of the biochemical and cellular mechanisms governing the host response (Hansen *et al.* 2006; Hauck *et al.* 2008). Subtle patterns of host response activation may arise where activation of protein systems (e.g. complement cascade, clot formation) and cell types (e.g. macrophages, lymphocytes, tissue cells) may overlap with cyto- and genotoxicity. For example, nanoparticulate materials may penetrate the intracellular space and induce cell death, leading to the indiscriminate liberation of biochemical signals that can exacerbate adverse reactions. Also, the penetration of these nanosized materials into the nuclear space may lead to genetic mutations and hence the arising of serious pathological conditions such as carcinogenesis (Hansen *et al.* 2006).

Before any cyto- or genotoxic event takes place, NP penetration into the body tissues is likely to induce the immune response by the host (Anderson 2001). This host response is a process triggered by the invasion of human tissues by a foreign body and involves the activation of biochemical (e.g. complement cascade) and cellular components of the immune system. MMs, immunocompetent cells derived from the blood mononuclear cell population, play a key role in this process. These cells are responsible for both the destruction and the clearance of the foreign body and for the secretion of important biochemical signals leading to immunosensitization (antigen-presenting cells). Furthermore, when inflammation is associated with tissue damage, MMs actively participate in the repair process by the secretion of growth factors (Martin & Leibovich 2005). In particular, these cells show a monocyte phenotype when they circulate in the blood stream and they transform into macrophages when they infiltrate tissues that have been either damaged and/or contaminated by foreign bodies (e.g. bacteria). However, especially during the early phases of activation, the distinction between these two phenotypes is subtle and difficult to distinguish and the cells are broadly defined as MMs.

During the early phases of inflammation, MMs acquire a pro-inflammatory phenotype that is devoted to phagocytose foreign bodies and tissue debris and to secrete pro-inflammatory factors such as the TNFα, which is able to recruit other inflammatory cells (Martin & Leibovich 2005). Later, monocytes may completely differentiate into macrophages to acquire a post-inflammatory phenotype and to secrete growth factors stimulating tissue formation by the induction of cell migration and proliferation (Martin & Leibovich 2005). In the last three decades, the use of medical implants made of synthetic materials (i.e. polymers, metals or ceramics) has opened new routes of

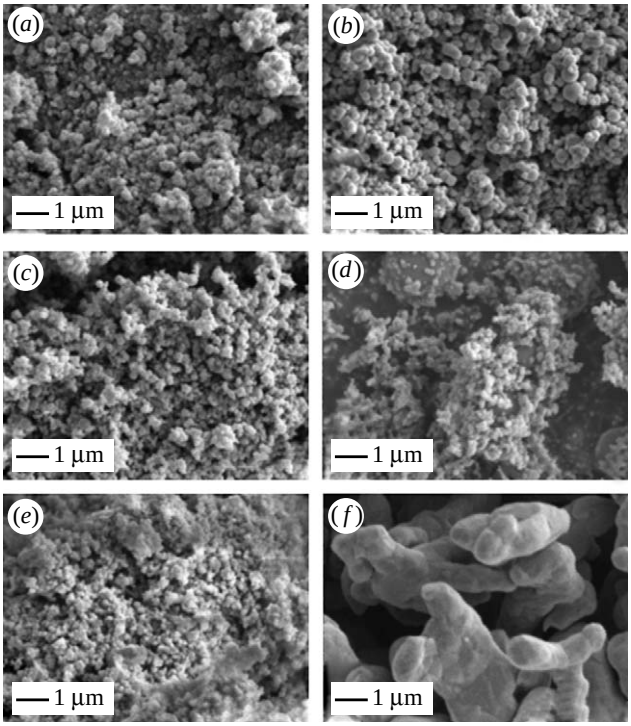

Figure 1. SEM analysis of NP. (*a*) Antimony NP, (*b*) silver NP, (*c*) titanium oxide NP, (*d*) nickel NP, (*e*) Fe_2O_3 NP and (*f*) cobalt NP. Micrographs were taken at 20 000× magnification. No significant morphological difference was observed between (*e*) Fe_2O_3 NP and Fe_3O_4 NP (data not shown).

investigation on the mechanisms controlling the inflammatory response (Mikhalovska *et al.* 2004; Santin *et al.* 2004; Harrison *et al.* 2007; Stewart *et al.* in press). For example, it has been shown that, when confronted by the relatively large size of the implant, macrophages enter the process known as 'frustrated phagocytosis' where the cells opt for fusing into giant cells, which are capable of walling off the foreign body (Anderson 2001). Later, the secretion of growth factors recruits tissue cells, the fibroblasts that form a more consistent fibrous tissue isolating the foreign material (Anderson 2001). The fibrous tissue is preceded by the deposition of granulation tissue. The granulation tissue is characterized by a high degree of vascularization that takes place through the formation of a dense network of capillaries. VEGF and PDGF-BB play an important role in the formation of both granulation and fibrous tissues (Harrison *et al.* 2007; Stewart *et al.* in press).

The *in vitro* model adopted in this work unveiled patterns of activation in the different components of the host response (i.e. fibrin clots, platelets and MMs) and related them to the different NP physico-chemical properties.

3.1. NP physico-chemical characterization

SEM of the different NP types confirmed that the size range was that reported by the manufacturer (table 1; figure 1*a–f*), with the exception of cobalt-based NP (figure 1*f*). These NPs were shown to be coalesced into aggregates of a size very close to or even above the macrophage phagocytosis limit.

Research in the field of biomedical implants has highlighted the important role played by proteins that, adsorbing on the surface of the foreign body, trigger macrophage activation (Anderson 2001; Santin *et al.* 2004; Martin & Leibovich 2005). It is now widely recognized that protein adsorption and macrophage activation depend on the physico-chemical properties of the material surface such as surface tension and roughness (Sanchez *et al.* 2008). Most of the NPs analysed in this work showed a relatively regular round-shaped morphology and a smooth surface. The antimony- and silver-based NPs had a very similar morphology with a relatively larger diameter and higher surface smoothness (figure 1*a–c*). The morphologies of the remaining NPs were still round-shaped, but they were characterized by a smaller diameter and by a relatively high level of surface roughness, especially if aggregated (figure 1*c*,*e*). The relatively low size of these NPs is expected to increase the exposed surface area of the foreign body, thus enhancing the level of protein adsorption and the consequent activation of macrophages. This biological process would be further amplified in those NPs that have either a rougher surface or aggregate into complexes still in the macrophage phagocytosis range. Among the NPs studied in this work, the iron-based NPs seem to meet these features. Conversely, in the case of Co-based NPs, their merging into branched structures of micrometric scale is likely to reduce the exposed surface area (figure 1*f*). Indeed, the ability of NPs to aggregate into larger structures when in the presence of body fluids may well lead to a different host response. However, the presence of artefacts generated by the sample preparation for SEM could not be ruled out.

3.2. Material-induced activation of host response components

To focus the study on the response of the MM to the different NP types, an experimental set-up was chosen where the freshly isolated mononuclear cells were left to adhere on PRP-conditioned surface and the non-adhering lymphocyte population was washed away after 3 hours of incubation. Immunostaining by CD68 antibody confirmed the MM phenotype of the adhering cells in both the absence (figure 2*a*) and presence of all the NP types (figure 2*b*). SEM analysis of both adhering MMs and platelets clearly showed differences in the activation of the host response components towards the different NPs. The cell morphology varied depending on the NP type (figure 3*a–n*). In particular, differences were observed in the degree of cell spreading and plasmalemma roughness. Control MMs not challenged by NPs were characterized by a relatively high degree of spreading on the TCP surface (figure 3*a*,*b*, thick arrows), while platelets appeared to assume a relatively round-shaped morphology with no sign of either aggregation or fragmentation, processes that take place during their activation (figure 3*a*,*b*, arrowheads).

In the chosen experimental protocol, to ensure the exposure of cells to the same amounts of NP ($0.05\ mg\ ml^{-1}$), NPs were added as the final step prior to 20 hours of incubation. The incubation of

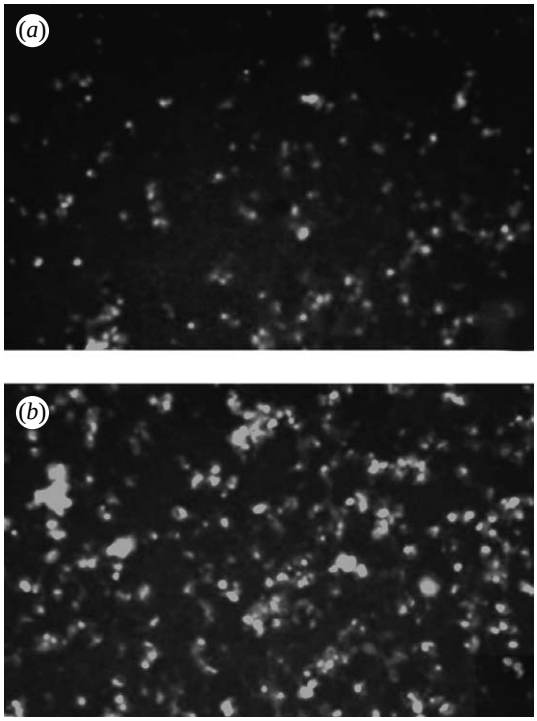

Figure 2. Typical CD68 immunostaining of adhering mononuclear cells in (*a*) a control experiment and (*b*) upon incubation with NP (TiO_2). The positive staining confirms the MM phenotype of the cells throughout the experiment.

NPs with MMs already adhering to the PRP preconditioned TCP seemed not to affect the ability of the elements of the host response to interact with the nanoparticulate foreign bodies. Fibrin clot, platelets and MMs responded to the different NP types, but in a different manner (figure 3*a*–*n*). Indeed, a pattern completely different from the control emerged from the SEM analysis of MMs incubated with antimony-based NPs (figure 3*c*,*d*). In the presence of this type of NP, MMs were shown to be entrapped in a fibrin clot (figure 3*c*,*d*, thin arrows) and assumed a round-shaped morphology with a plasmalemma characterized by small and very dense protrusions typical of an activated monocyte phenotype (figure 3*c*,*d*, thick arrows). Platelets showed extensive aggregation and appeared to be entrapped and interacting with the fibrin mesh, resembling a typical blood clot (figure 3*d*, arrowheads and thin arrows). Antimony-based NPs appeared to be mainly distributed into the extracellular space and in preferential contact with fibrin fibres, sometimes aligned along the fibre axis, but mostly embedded as aggregates in fibrin cross-linking domains (figure 3*d*, thin arrows). Silver NP led to a morphological pattern similar to antimony, but fibrin polymerization and platelet aggregation were less pronounced (figure 3*e*,*f*, thin arrows and arrowheads). MM morphology was still relatively round-shaped (figure 3*e*,*f*, thick arrows), but the lower density of the fibrin mesh allowed the cells to establish direct contact with the plasma-preconditioned TCP surface and to acquire morphology typical of an activated macrophage and similar to that of MMs adhering on control TCP. Well-established filopodia and a rough plasmalemma were visible in most of these adhering cells. As for antimony, silver-based NPs were mainly observed in the extracellular space (figure 3*e*) and entrapped as aggregates at fibrin cross-linking points (figure 3*f*, thin arrow). In the case of nickel-based NPs, a morphological pattern similar to silver was observed in all the analysed components (figure 3*g*,*h*). However, MM (thick arrows) and platelet (arrowheads) densities were lower and the deposition of cross-linked fibrin fibres was also less pronounced (figure 3*g*). High-magnification micrographs highlighted that both MMs and platelets were preferentially interacting with cross-linked fibrin fibre domains and showed no significant presence of NP in the extracellular space (figure 3*h*).

A completely different pattern emerged when MMs were incubated with titanium oxide NP (figure 3*i*,*j*, thick arrows). Here, most of the cells acquired a high degree of spreading on the TCP and presented a smooth plasmalemma. However, MMs were also shown to extend filopodia, which protruded from the main cell body to reach and make contact with titanium oxide NP. Where NP aggregates assumed a relatively large size, MMs appeared to surround and engulf them, but still maintaining a relatively smooth plasmalemma (figure 3*j*). Smooth and isolated platelets were also visible and no fibrin polymerization could be observed (figure 3*i*,*j*, arrowheads).

The two types of iron-based NPs led to a complete MM spreading on the TCP surface and to their fusion into giant cells. Spreading and fusion were so pronounced that they made cell identification on the plastic surface difficult (figure 3*k*,*l*, thick arrows). The interaction of both MMs and aggregating platelets with the iron-based NPs was also visible (figure 3*l*, arrowhead). Iron-based NPs appeared to be internalized by the cells when isolated, but left in the extracellular space when aggregated (figure 3*k*). Platelets were only marginally involved in the host response.

Cobalt-based NPs led to a similar pattern where MMs were completely spread and showed internalized NPs (figure 3*m*,*n*, thick arrows). However, MM density as well as their tendency to fuse into giant cells was relatively lower than iron-based NPs. However, platelets appeared mostly isolated and spread with no significant aggregation or fragmentation (figure 3*m*,*n*, arrowheads). These data were unexpected as the relatively large dimension of the cobalt-based NPs (figure 1*f*) was thought to lead to MM-frustrated phagocytosis. However, it has to be noted that NP aggregates were only rarely found (figure 3*n*) and that NPs of smaller scale seemed to be present. It may be speculated that the relatively larger particles were left in the extracellular space and washed off during the sample preparation for SEM.

Rhodamine–phalloidin staining contributed to the study of MM and platelet distribution and their degree of interaction (figure 4*a*–*h*). Overall, the pattern observed by SEM was confirmed. In addition, the relatively low magnification of the micrographs (20×) showed both the relatively different density of adhering cells when exposed to the different NPs and their different patterns of adhesion. In particular, antimony seemed to show a relatively higher cell density that was uniformly dispersed across the surface

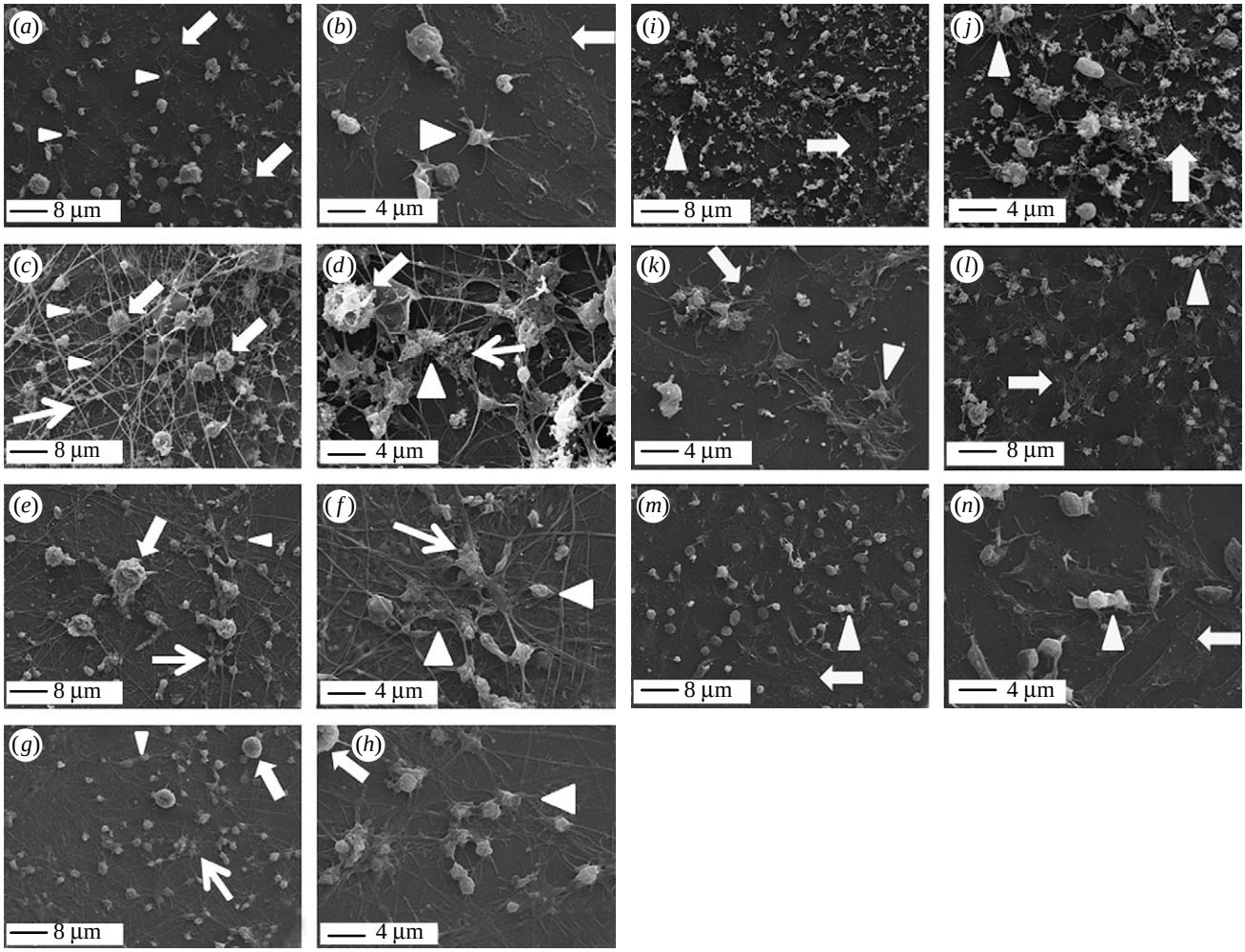

Figure 3. SEM analysis of the effect of NPs on components of the host response. (*a*,*b*) Control TCP, (*c*,*d*) antimony NP, (*e*,*f*) silver NP, (*g*,*h*) nickel NP, (*i*,*j*) titanium oxide NP, (*k*,*l*) iron NP and (*m*,*n*) cobalt NP. (*a*–*h*) 2000× magnification; (*i*–*n*) 5000× magnification. Thick arrows, MM; arrowheads, platelets; thin arrows, polymerized fibrin fibrils and cross-linking points.

(figure 4*b*). All the other NP types showed cell densities similar to the control and the tendency to form clusters (figure 4*c*–*h*).

The evident effect of antimony-, silver- and nickel-based NPs on the clotting system deserves particular consideration if it is considered that in the adopted experimental model the material was pre-conditioned with human plasma that was derived from heparin-treated blood. Regardless of the presence of this anti-coagulant agent, the plasma proteins adsorbed onto the material surface appeared to initiate the polymerization of the fibrin and its cross-linking into a mesh. When this process was accentuated (i.e. antimony-based NPs), a tri-dimensional mesh could be observed and NPs seemed to be more concentrated in the areas of fibrin fibril cross-linking, supporting their possible role as catalysts of clot activation by contact. Indeed, clot activation by contact with the surface of a foreign material is a known phenomenon and has been widely proven in the field of biomedical implants as a consequence of fibrinogen and fibrin adsorption onto surfaces (Hunt *et al.* 1997; Mikhalovska *et al.* 2004; Sanchez *et al.* 2008). The experimental conditions of this study do not discriminate between the sequences of events leading to fibrin polymerization. More explicitly, it is not possible to understand whether fibrin polymerization and its cross-linking were induced by areas of relatively higher NP density or fibrin polymerization led to the accumulation of NPs in areas of fibril tight apposition. However, it can be speculated that, regardless of their chemical nature, NPs with a relatively regular round-shaped morphology and high surface smoothness (antimony- and silver-based NPs) were favouring a higher level of fibrin clot formation. It may be suggested that, in the case of significant penetration of NPs based on antimony, silver and nickel into the vascular tree or into highly vascularized organs such as lungs and liver, undesired blood clot can form, leading to thrombus development.

The samples showing the formation of a fibrin clot also affected the behaviour of platelets and MMs; they showed a preferential adhesion to the fibrin clot rather than to the TCP surface. As a consequence, the morphology of both platelets and MMs was different from those incubated with the other NPs. It is likely that, as the fibrin mesh is the main component of the blood clot, MMs may recognize it as the natural substrate they face after tissue damage, thus preferring it to the underlying TCP surface. Conversely, when no significant fibrin clot was formed, a preferential interaction with the TCP surface was established. In this case, MMs spread on the plastic surface in

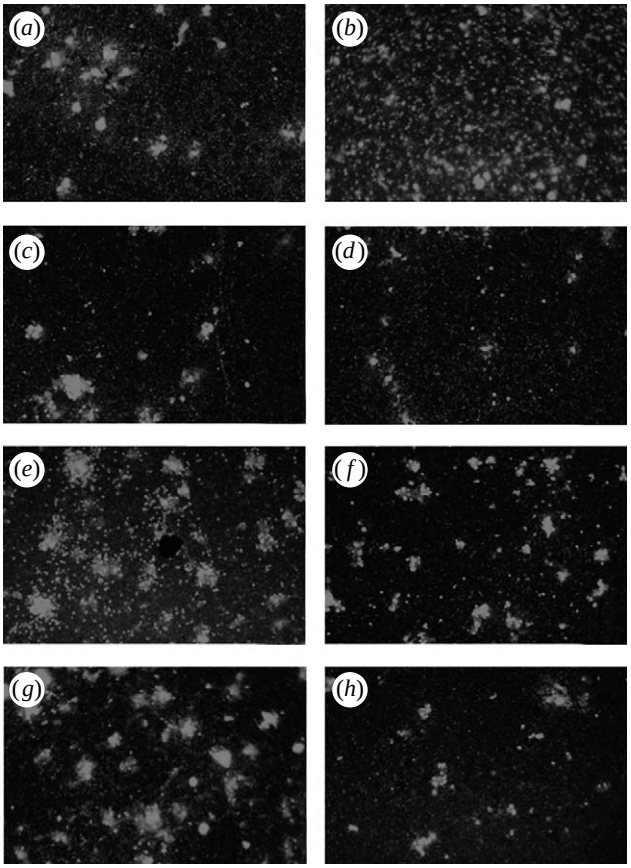

Figure 4. Rhodamine–phalloidin staining of adhering MMs. (*a*) Control TCP, (*b*) antimony NP, (*c*) silver NP, (*d*) nickel NP, (*e*) Fe_3O_4 NP, (*f*) Fe_2O_3 NP, (*g*) TiO_2 NP and (*h*) cobalt NP. Photos were taken at 20× magnification to show differences in both relative cell density and patterns of adhesion.

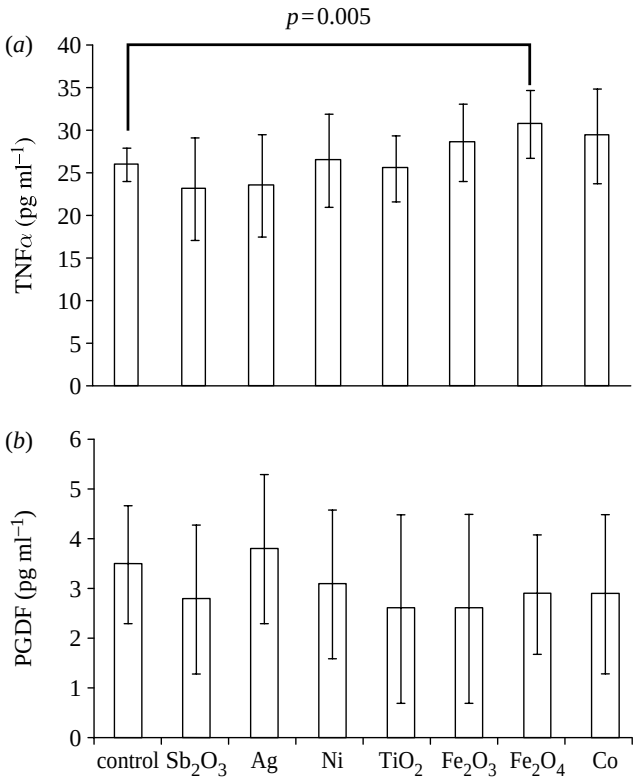

Figure 5. Growth factor secretion by MMs incubated with NPs after 20 h incubation. (*a*) TNFα and (*b*) PDGF-BB. Data were transformed by subtracting the blank (FCS-enriched DMEM) absorbance readings from the sample readings.

a manner similar to that of the control samples, although with different degrees of spreading depending on the NP type. The relatively high degree of spreading of these cells allowed the detection of NPs internalized in their cytoplasm (figure 3*k*,*n*). Furthermore, they also showed the tendency to fuse into giant cells as they would do in the presence of a foreign material of large size. It can be speculated that both in control and NPs based on cobalt, iron and titanium, MMs sensed the TCP plastic surface more than the effect of the NPs. However, the effect of the latter on the inflammatory cell activation was also evident as the cells tended to extend their filopodia towards the NPs and to surround them when in an aggregated state.

In this study, three specific growth factors were considered. The TNFα was tested as a marker of MM pro-inflammatory phenotype, while the PDGF-BB and the VEGF were assessed as promoters of granulation and fibrous tissue formation. Indeed, these growth factors are known to be potent stimulators of angiogenesis (VEGF) and fibroblast migration and blood vessel consolidation (PDGF-BB).

The secretion of a pro-inflammatory cytokine such as the TNFα clearly showed a trend consistent to the SEM findings (figure 5*a*). In particular, the three types of NP, which were internalized by cells with a relatively high degree of cell spreading, were also observed to secrete higher levels of this cytokine. In particular, Fe_3O_4-based NPs showed a significantly higher secretion of this pro-inflammatory factor (paired *t*-test, $p=0.005$), while Fe_2O_3- and Co-based NPs showed a non-significant increase. Setting the experiment with an initially higher cell seeding density or with longer incubation times might have made these differences statistically significant. The remaining NPs showed TNFα secretion levels similar to those of control cells. However, as cell numbers were not evaluated, the higher levels of TNFα observed in the case of cobalt-, iron- and titanium-based NPs could be due to higher cell proliferation upon exposure to the different NPs and not to higher levels of activation. If this was the case, it is still noticeable that these three types of NP can lead to higher cell proliferation and, therefore, to higher TNFα release levels. It can also be speculated that metal NPs may release metal ions that are known to affect markedly cell activity (Lucarelli *et al.* 2004; Keegan *et al.* 2008).

Conversely, all the NP samples showed release levels of PDGF-BB (figure 5*b*) and VEGF (data not shown) very close to the assay's lower sensitivity threshold and comparable to the control cells (data not shown). Previous work has shown that MMs are stimulated to produce relatively high levels of PDGF-BB when adhering on stainless steel surfaces, which are composed of iron, nickel and cobalt (Harrison *et al.* 2007; Stewart *et al.* in press). Therefore, these data seem to suggest that the analysed NPs were not able to activate MM biochemical pathways favouring granulation and fibrous tissue formation and that materials with similar chemistry can completely change their effects

Table 2. NP cytotoxic potential assessed as LDH activity.

sample	LDH activity (arb. unit)	±s.d.
positive control[a]	1.02	0.14
negative control	0.24	0.09
Sb_2O_3	0.29	0.13
silver	0.27	0.04
nickel	0.28	0.10
TiO_2	0.31	0.17
cobalt	0.27	0.19
Fe_2O_3	0.23	0.08
Fe_3O_4	0.29	0.16

[a]Cells undergoing lytic cycle by Triton-X100 treatment.

on MMs depending on their overall physico-chemical characteristics (e.g. morphology and aggregation).

LDH activity was measured to assess whether the released levels of TNFα were due to cell activation or as a consequence of loss of cell membrane integrity due to cytotoxicity. The NP-induced LDH values were not significantly different from the negative control (0.24 ± 0.09 LDH arbitrary unit), suggesting no significant NP cytotoxicity (table 2). The lack of cytotoxicity is corroborated both by the relatively higher cell densities found in samples spiked with NPs and by the healthy morphology of the cells as highlighted by SEM. It has also to be outlined that, in the chosen experimental model, MMs were challenged by concentrations of NP which may be significantly higher than those reached in most medical or environmental scenarios.

Regardless of its limitations, the adopted *in vitro* model has shown that the penetration of the various types of NP into tissues and organs may direct the host response components towards specific biochemical pathways.

4. CONCLUSION

The present study shows that the nature of the NP material released from environmental sources, implant wear or nanomedicine intervention can have an impact on various aspects of the host response, leading to pathological complications. For example, the accumulation of clot-inducing NPs in blood vessels may induce thrombosis, while the accumulation of pro-inflammatory NPs in vital and highly vascularized organs such as lungs and liver may lead to serious structural damage and homeostasis alterations. Finally, although no significant cell death by NPs was observed under the experimental conditions of this study, subtle cytotoxic and genotoxic effects not investigated in this work may not be ruled out when MMs are exposed to nanoparticulate materials for prolonged periods of time.

The study was approved by the University of Brighton local research ethics committee.

REFERENCES

Anderson, J. M. 2001 Biological responses to materials. *Ann. Rev. Mater. Res.* **31**, 81–110. (doi:10.1146/annurev.matsci.31.1.81)

Frias, J. C., Ma, Y., Williams, K. J., Fayad, Z. A. & Fisher, E. A. 2006 Properties of a versatile nanoparticle platform contrast agent to image and characterize atherosclerotic plaques by magnetic resonance imaging. *Nano. Lett.* **6**, 2220–2224. (doi:10.1021/nl061498r)

Frias, J. C., Lipinski, M. J., Albelda, M. T., Ibáñez, B., Soriano, C., García-España, E., Jiménez-Borreguero, L. J. & Badimon, J. J. 2008 Nanoparticles as contrast agents for MRI of atherosclerotic lesions. *Clin. Med. Card.* **173**, 173–179.

Hansen, T., Clermont, G., Alves, A., Eloy, R., Brochhausen, C., Boutrand, J. P., Gatti, A. M. & Kirkpatrick, C. J. 2006 Biological tolerance of different materials in bulk and nanoparticulate form in a rat model: sarcoma development by nanoparticles. *J. R. Soc. Interface* **3**, 767–775. (doi:10.1098/rsif.2006.0145)

Harrison, M., Siddiq, M. A., Guildford, A., Bone, A. & Santin, M. 2007 Stent material surface and glucose activate mononuclear cells of control, type 1 and type 2 diabetes subjects. *J. Biomed. Mater. Res.* **83A**, 52–57. (doi:10.1002/jbm.a.31204)

Hauck, T. S., Ghazani, A. A. & Chan, W. C. W. 2008 Assessing the effect of surface chemistry on gold nanorod uptake, toxicity, and gene expression in mammalian cells. *Small* **4**, 153–159. (doi:10.1002/smll.200700217)

Hunt, B. J., Parrat, R., Cable, M., Finch, D. & Yacoub, M. 1997 Activation of coagulation and platelets is affected by the hydrophobicity of artificial surfaces. *Blood Coagul. Fibrinol.* **8**, 223–231. (doi:10.1097/00001721-199706000-00003)

Kagan, V. E., Bayir, H. & Shvedova, A. A. 2005 Nanomedicine and nanotoxicology: two sides of the same coin. *Nanomed. Nanotech. Biol. Med.* **1**, 313–316. (doi:10.1016/j.nano.2005.10.003)

Keegan, G. M., Learmonth, I. D. & Case, C. P. 2008 A systematic comparison of the actual, potential, and theoretical health effects of cobalt and chromium exposures from industry and surgical implants. *Crit. Rev. Toxicol.* **38**, 645–674. (doi:10.1080/10408440701845534)

Kelly, K. A., Allport, J. R., Tsourkas, A., Shinde-Patil, V. R., Josephson, L. & Weissleder, R. 2005 Detection of vascular adhesion molecule-1 expression using a novel multimodal nanoparticle. *Circ. Res.* **96**, 327–336. (doi:10.1161/01.RES.0000155722.17881.dd)

Kooi, M. E., Cappendijk, V. C., Cleutjens, K. B. J. M., Kessels, A. G. H., Kitslaar, P. J. E. H., Borgers, M., Frederik, P. M., Daemen, M. J. A. P. & van Engelshoven, J. M. A. 2003 Accumulation of ultrasmall superparamagnetic particles of iron oxide in human atherosclerotic plaques can be detected by *in vivo* magnetic resonance imaging. *Circulation* **107**, 2453–2458. (doi:10.1161/01.CIR.0000068315.98705.CC)

Lewinski, N., Colvin, V. & Drezek, R. 2008 Cytotoxicity of nanoparticles. *Small* **4**, 26–49. (doi:10.1002/smll.200700595)

Lucarelli, M., Gatti, A. M., Savarino, G., Quattroni, P., Martinelli, L., Monari, E. & Boraschi, D. 2004 Innate defence functions of macrophages can be biased by nano-sized ceramic and metallic particles. *Eur. Cytok. Net.* **15**, 339–346.

Martin, P. & Leibovich, S. J. 2005 Inflammatory cells during wound repair: the good, the bad and the ugly. *Trends Cell Biol.* **15**, 599–607. (doi:10.1016/j.tcb.2005.09.002)

McAteer, M. A., Sibson, N. R., von Zur Muhlen, C., Schneider, J. E., Lowe, A. S., Warrick, N., Channon, K. M., Anthony, D. C. & Choudhury, R. P. 2007 *In vivo* magnetic resonance imaging of acute brain inflammation using microparticles of iron oxide. *Nat. Med.* **13**, 1253–1258. (doi: 10.1038/nm1631)

Mikhalovska, L. I., Santin, M., Denyer, S. P., Lloyd, A. W., Teer, D. G., Field, S. & Mikhalovsky, S. 2004 Fibrinogen

adsorption and platelet adhesion to metal and carbon coatings. *Thromb. Haemost.* **92**, 1032–1039. (doi:10.1160/TH04-03-0171)

Sanchez, J., Elgue, G., Larsson, R., Nilsson, B. & Olsson, P. 2008 Surface-adsorbed fibrinogen and fibrin may activate the contact activation system. *Thromb. Res.* **122**, 257–263. (doi:10.1016/j.thromres.2007.11.008)

Santin, M., Mikhalovska, L., Lloyd, A. W. & Mikhalovsky, S. 2004 *In vitro* host response assessment of biomaterials for cardiovascular stent manufacture. *J. Mater. Sci. Mater. Med.* **15**, 473–477. (doi:10.1023/B:JMSM.0000021123.51752.11)

Stewart, H. J. S., Guildford, A. L., Lawrence-Watt, D. J. & Santin, M. In press. Substrate induced phenotypical change of monocytes/macrophages into myofibroblast-like cells: a new insight into the mechanism of in-stent restenosis. *J. Biomed. Mater. Res. A.* (doi:10.1002/jbm.a.32100)

van Zur Muhlen, C., von Elverfeldt, D., Bassler, N., Neudorfer, I., Steitz, B., Petri-Fink, A., Hofmann, H., Bode, C. & Peter, K. 2006 Superparamagnetic iron oxide binding and uptake as imaged by magnetic resonance is mediated by the integrin receptor Mac-1 (CD11b/CD18): implications on imaging of atherosclerotic plaques. *Atherosclerosis* **193**, 102–111. (doi:10.1016/j.atherosclerosis.2006.08.048)